THE JOURNAL OF BIOLOGICAL CHEMISTRY VOL. 289, NO. 23, pp. 16100–16113, June 6, 2014

Isoform-selective Inhibition of Facilitative Glucose Transporters

*ELUCIDATION OF THE MOLECULAR MECHANISM OF HIV PROTEASE INHIBITOR BINDING**

Received for publication, October 22, 2013, and in revised form, March 28, 2014 Published, JBC Papers in Press, April 4, 2014, DOI 10.1074/jbc.M113.528430

Richard C. Hresko[‡], Thomas E. Kraft[‡], Anatoly Tzekov[‡], Scott A. Wildman[§], and Paul W. Hruz[‡¶1]

From the Department of [‡]Pediatrics, [§]Biochemistry, and [¶]Cell Biology and Physiology, Washington University School of Medicine, St. Louis, Missouri 63110

Background: The structural features in GLUT4 that confer selective binding and inhibition by HIV protease inhibitors (PIs) are unknown.
Results: Substitution of amino acid residues in transmembrane helices 1 and 5 between GLUTs 1 and 4 alters indinavir binding and effects on transport activity.
Conclusion: Thr-30 and His-160 hinder the binding of PIs to GLUT1.
Significance: These data provide a means to design isoform-selective GLUT antagonists.

Pharmacologic HIV protease inhibitors (PIs) and structurally related oligopeptides are known to reversibly bind and inactivate the insulin-responsive facilitative glucose transporter 4 (GLUT4). Several PIs exhibit isoform selectivity with little effect on GLUT1. The ability to target individual GLUT isoforms in an acute and reversible manner provides novel means both to investigate the contribution of individual GLUTs to health and disease and to develop targeted treatment of glucose-dependent diseases. To determine the molecular basis of transport inhibition, a series of chimeric proteins containing transmembrane and cytosolic domains from GLUT1 and GLUT4 and/or point mutations were generated and expressed in HEK293 cells. Structural integrity was confirmed via measurement of *N*-[2-[2-[2-[(*N*-biotinylcaproylamino)ethoxy)ethoxyl]-4-[2-(trifluoromethyl)-3*H*-diazirin-3-yl]benzoyl]-1,3-bis(mannopyranosyl-4-yloxy)-2-propylamine (ATB-BMPA) labeling of the chimeric proteins in low density microsome fractions isolated from stably transfected 293 cells. Functional integrity was assessed via measurement of zero-trans 2-deoxyglucose (2-DOG) uptake. ATB-BMPA labeling studies and 2-DOG uptake revealed that transmembrane helices 1 and 5 contain amino acid residues that influence inhibitor access to the transporter binding domain. Substitution of Thr-30 and His-160 in GLUT1 to the corresponding positions in GLUT4 is sufficient to completely transform GLUT1 into GLUT4 with respect to indinavir inhibition of 2-DOG uptake and ATB-BMPA binding. These data provide a structural basis for the selectivity of PIs toward GLUT4 over GLUT1 that can be used in ongoing novel drug design.

Facilitative glucose transport in mammalian cells is mediated by the SLC2A family of tissue-specific membrane glycoproteins (glucose transporters (GLUTs)).[2] The erythrocyte transporter GLUT1, which is ubiquitously expressed and generally serves to mediate basal glucose transport, is the most extensively characterized GLUT (1). Regulation of the insulin-responsive facilitative glucose transporter GLUT4 has been intensively studied in relation to the pathophysiology of type 2 diabetes mellitus (2). Although collectively the GLUT proteins share less than 40% sequence identity, all are predicted to share similar membrane topologies with high homology within putative TM domains. Despite the cloning of GLUTs over a quarter century ago, a full understanding of the molecular mechanisms responsible for the function of these important TM proteins has remained elusive. GLUT structure has been inferred by a number of mutagenesis and labeling studies, but to date, no crystal structure is available for any of the GLUTs. Each of the GLUTs is predicted to contain 12 TM α-helices with both the amino and carboxyl termini within the cytoplasm (3).

The HIV protease inhibitor (PI) indinavir is known to acutely inhibit GLUT4 activity via reversible binding to the endofacial surface of the transporter (4, 5). Although indinavir acts as an antagonist of GLUT4 at therapeutically relevant drug levels (5–10 μM), within this concentration range, the drug has little effect on GLUT1 activity (6). In addition to providing insight into the etiology of insulin resistance in HIV-infected patients receiving this class of drugs (7) and assisting in the development of safer PIs (8), the selectivity of indinavir as a GLUT4 antagonist over GLUT1 has been used to determine the relative activity of these transporter isoforms in insulin-responsive tissues (9).

Subsequent studies have revealed that PIs have differing affinities for GLUT1 and GLUT4 (5) with many of the newer

* This work was supported, in whole or in part, by National Institutes of Health Grants DK064572 and HL092798.
[1] To whom correspondence should be addressed: Dept. of Pediatrics, Washington University School of Medicine, 660 S. Euclid Ave., Campus Box 8208, St. Louis, MO 63110. Tel.: 314-286-2797; Fax: 314-286-2892; E-mail: hruz_p@kids.wustl.edu.

[2] The abbreviations used are: GLUT, glucose transporter; Ahx, aminohexanoic acid; ATB-BMPA, *N*-[2-[2-[2-[(*N*-biotinylcaproylamino)ethoxy)ethoxyl]-4-[2-(trifluoromethyl)-3*H*-diazirin-3-yl]benzoyl]-1,3-bis(mannopyranosyl-4-yloxy)-2-propylamine; Bpa, *p*-benzoyl-L-phenylalanine; CB, cytochalasin B; DMSO, dimethyl sulfoxide; DOG, deoxyglucose; HR-1, Z-HFF-Bpa-Ahx-Ahx-DYDDDDK; LDM, low density microsome; PI, protease inhibitor; PM, plasma membrane; TM, transmembrane; XylE, xylose transporter; Z, oxybenzylcarbonyl; Z-HFFe, oxybenzylcarbonyl-His-Phe-Phe-*O*-ethyl ester; CH, chimera.

agents having minimal effect on glucose transport (8, 10). Recognition that all first generation PIs contain a peptidomimetic core structure led to our identification of several hydrophobic oligopeptides exhibiting similar selectivity and potency as GLUT4 antagonists (11). The unique structural features present in GLUT4 that confer susceptibility to binding and inactivation by indinavir, however, remain unknown.

The membrane-impermeant bismannose-containing photolabel *N*-[2-[2-[2-[(*N*-biotinylcaproylamino)ethoxy)ethoxyl]-4-[2-(trifluoromethyl)-3*H*-diazirin-3-yl]benzoyl]-1,3-bis(mannopyranosyl-4-yloxy)-2-propylamine (ATB-BMPA) can inhibit sugar transport by binding to the glucose binding site accessed from the exofacial side and has been extensively used to quantify cell surface levels of the GLUT proteins (12). Our laboratory has recently demonstrated that ATB-BMPA can also be used to label GLUTs in low density microsomes (LDMs) where the transporter orientation is inverted relative to that found in the plasma membrane (PM) (13). Chimeric glucose transporters in which structural domains from different GLUTs are interchanged have been shown previously to maintain structural and functional activity (14–16). Because several PIs including indinavir selectively inactivate GLUT4 over GLUT1, we hypothesized that the generation of GLUT1/GLUT4 chimeric transporters would assist efforts to identify the PI binding site in GLUT4. Here we report evidence for the involvement of Thr-30 in TM helix 1 and His-160 in TM helix 5 as amino acid residues important in hindering the susceptibility of GLUT1 to inhibition by PIs.

EXPERIMENTAL PROCEDURES

Materials—2-Deoxy[^{3}H]glucose, cytochalasin B (CB), and all oligonucleotides were purchased from Sigma. Crixivan (indinavir) was obtained from Merck. Oxybenzylcarbonyl-His-Phe-Phe-*O*-ethyl ester (Z-HFFe) was purchased from Bachem (King of Prussia, PA). Z-HFF-Bpa-Ahx-Ahx-DYDDDDK (HR-1) where Bpa is *p*-benzoyl-L-phenylalanine and Ahx is aminohexanoic acid was synthesized by Anaspec (San Jose, CA). 3T3-L1 fibroblasts and HEK293 cells were acquired from the American Type Culture Collection. 293GPG packaging cells were a kind gift from Dan Ory (Washington University, St. Louis, MO). PEG-biotin cap-ATB-BMPA was purchased from Toronto Research Chemicals, Inc. (Ontario, Canada). GLUT1 polyclonal antibody directed against the carboxyl terminus was a kind gift from Mike Mueckler (Washington University, St. Louis, MO). GLUT4 antibody was custom produced by Invitrogen using a peptide corresponding to the 16 carboxyl-terminal residues of GLUT4.

Construction of GLUT1/GLUT4 Chimeras—CH 1-444, CH 4-111, 14-half CH, and 41-half CH chimeric transporters were made using established polymerase chain reaction (PCR) methodologies. A Myc tag sequence (AEEQKLISEEDLLK) was incorporated into the first exofacial domain of both rat GLUT1 (after Ile-56) and rat GLUT4 (after Pro-60), and a six-histidine sequence was inserted at the extreme carboxyl terminus of both transporters using a PCR-based gene assembly approach. PCR products were gel-purified, cloned into a TOPO TA cloning vector, and sequence-verified. Myc-GLUT1-His and Myc-GLUT4-His were then used as templates to generate glucose transporter fragments by PCR. The PCR products were gel-purified and combined in an equal molar ratio with a set of "band-aid" primers to generate a template mixture. Each band-aid primer consists of ~40 bases. Half of it anneals to the 3′-end of one GLUT fragment, and the other half anneals to the 5′-end of a second fragment to be assembled together. An amino terminus-specific forward primer and a carboxyl terminus-specific reverse primer were used at 10 pmol/50-μl reaction to assemble each chimera. To aid in downstream cloning, vector-specific restriction sites were inserted into these primers. Myc-GLUT1-His, Myc-GLUT4-His, and the chimeric transporters were then subcloned into the retroviral mammalian expression vector ΔU3nlsLacZ (17). The exchange of a single helical or linker domain from one GLUT isoform to another was carried out using a two-stage PCR procedure (18) based on the QuikChange site-directed mutagenesis protocol from Agilent Technologies (La Jolla, CA). All chimeras were completely sequenced. A QuikChange II XL site-directed mutagenesis kit (Agilent Technologies) was used to correct any uncovered point mutations and to generate Myc-GLUT-His point mutants.

293GPG Packaging Cell Transfection and Retroviral Infection—293GPG cells were plated in 60-mm dishes in Dulbecco's modified Eagle's medium (DMEM) supplemented with 10% fetal bovine serum (FBS), 2 mM L-glutamine, 100 IU/ml penicillin, 0.1 mg/ml streptomycin, 1 μg/ml tetracycline, 2 μg/ml puromycin, and 0.3 mg/ml geneticin. Cells at 30–50% confluence were transiently transfected with 2 μg of Myc-GLUT-His/ΔU3nlsLacZ DNA using Optifect reagent (Invitrogen). After 24 h, the transfection medium was replaced with 4 ml of growth medium (DMEM containing 10% FBS, 2 mM glutamine, 100 IU/ml penicillin, and 0.1 mg/ml streptomycin). 48 h later, virus was harvested and used to infect a 10-cm plate of HEK293 cells (30–50% confluent) using the following procedure. 2 ml of fresh growth medium was mixed in a 15-ml conical tube with 6 μl of the cationic polymer Polybrene (10 mg/ml) and 2 ml of medium harvested from the virus-producing 293GPG cells. Medium was removed from the HEK293 cells and replaced with the 4 ml of medium from the conical tube. 24 h postinfection, the virus-containing medium was replaced with 9 ml of fresh growth medium. Expression of Myc-GLUT-His protein was subsequently tested by immunoblot analysis using a c-Myc (9E10) antibody (Santa Cruz Biotechnology).

2-Deoxyglucose Uptake Measurements in HEK293 Cells—HEK293 cells overexpressing Myc-GLUT-His constructs were grown to confluence in growth medium. The uptake of 2-deoxy[^{3}H]glucose (50 μM) was measured in Krebs-Ringer phosphate buffer for 6 min at 37 °C as described previously (19). Indinavir (50 μM), Z-HFFe (100 μM), HR-1 (100 μM), and CB (20 μM) were added 6 min prior to the start of the reaction.

Isolation of Low Density Microsomes—3T3-L1 fibroblasts were differentiated into adipocytes as described previously (19). LDMs were obtained from fully differentiated adipocytes as reported previously (20). The same procedure was used to isolate LDMs from HEK293 cells.

Photolabeling of LDMs—Inhibitors were added to LDMs (200–400 μg) for 10 min at room temperature. Samples (final volume, 110 μl) were then incubated for 10 min at room tem-

perature with biotinylated ATB-BMPA (50 μM final concentration) or HR-1 (2.5 μM final concentration) and then placed on ice prior to UV irradiation. Reactions were transferred to a 24-well low protein retention culture dish (Costar, Corning, NY) and then irradiated at room temperature 5 cm from a Green Spot UV lamp for 1 min (30 s of light followed by 30 s of darkness followed by 30 s of light).

Isolation and Quantification of Labeled GLUT1 and GLUT4 Proteins from LDMs of 3T3-L1 Adipocytes—20 μl of bovine serum albumin (1.5 mg/ml final concentration) was added to the UV-irradiated samples in a siliconized Eppendorf tube. Excess biotinylated ATB-BMPA label or FLAG-tagged HR-1 was removed using a 0.5-ml Zeba spin desalting column (Pierce). Membranes were solubilized for 30 min at 4 °C with 2% Thesit detergent in 25 mM phosphate and 100 mM NaCl, pH 7.4 buffer containing protease inhibitors followed by the removal of insoluble material by centrifugation at 16,000 $\times$ *g* for 10 min. Biotinylated and FLAG-tagged proteins were isolated from the Thesit-solubilized LDMs using either 50 μl of high capacity streptavidin-agarose resin (Pierce) or 50 μl of α-FLAG affinity gel (Sigma), respectively. Proteins were eluted from the washed resin with 2$\times$ Laemmli sample buffer. To remove the biotinylated proteins from the streptavidin resin, Laemmli buffer samples were heated at 95 °C for 20 min. Eluted proteins were analyzed by immunoblot analysis using GLUT1- and GLUT4-specific antibodies and quantified using an Odyssey infrared imaging system (LI-COR Biosciences, Lincoln, NE).

Isolation of Myc-GLUT-His Proteins and Quantification of the Amount of Transporter Labeled with ATB-BMPA—LDMs from HEK293 cells overexpressing Myc-GLUT-His transporters were UV-irradiated with biotinylated ATB-BMPA and solubilized with Thesit detergent buffer exactly as described above for the 3T3-L1 adipocytes. Myc-GLUT-His proteins were isolated from the solubilized LDMs using 50 μl of Protein G Plus-agarose (Pierce) precoupled with 5 μg of c-Myc (9E10) antibody (Santa Cruz Biotechnology). Immunoprecipitates were analyzed by immunoblot analysis using fluorescently labeled streptavidin (LI-COR Biosciences) and a GLUT-specific antibody and then quantified using the Odyssey infrared imaging system. The ratio of streptavidin to GLUT protein represents the fraction of immunoprecipitated Myc-GLUT-His protein labeled with biotinylated ATB-BMPA.

Modeling of Indinavir Binding to GLUT4—GLUT4 models are based on sequence alignments with major facilitator superfamily transporters XylE (Protein Data Bank code 4GBZ) for the outward open conformation and *Staphylococcus epidermidis* glucose/H^+ symporter (Protein Data Bank code 4LDS) for the inward open conformation using ClustalΩ (21) and PFAAT (22). A homology model of the TM helices was done using Molecular Operating Environment (MOE 2013.08) (Chemical Computing Group Inc., Montreal, Canada). The structure of helix 1 is taken from Protein Data Bank code 4GBZ for both conformations because Protein Data Bank code 4LDS shows a significant bend allowed by the shorter construct used. The helix is expected to be straighter in GLUT4 with a longer terminal tail. The loops were modeled separately based on the same two template structures. All modeling was done in a phospholipid bilayer, and the final structures were refined using the AMBER99SB force field. Indinavir was docked to GLUT4 modeled structures using AutoDock Vina (23) and visualized using PyMOL Molecular Graphics System Version 1.5.0.4 (Schrödinger, LLC.)

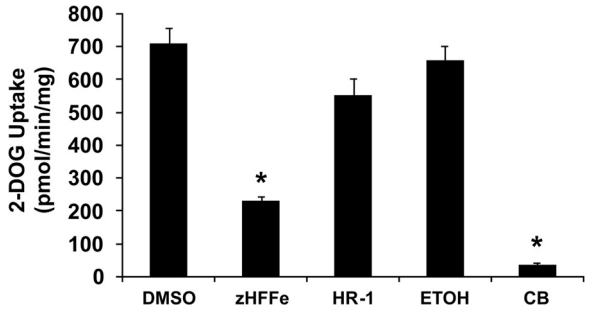

FIGURE 1. **Inhibition of 2-deoxyglucose uptake by Z-HFF peptides in HEK293 cells overexpressing GLUT4.** Z-HFFe and HR-1 peptides (100 μM final concentration) prepared in DMSO were added 6 min prior to measuring 2-deoxy[^{3}H]glucose uptake (50 μM; 6 min at 37 °C). Inhibition with 20 μM CB prepared in ethanol (*ETOH*) is shown for comparison. Data are expressed as mean uptakes ($n = 3$). *Error bars* represent S.E. *, $p < 0.05$ *versus* vehicle control.

Statistical Analysis—ATB-BMPA binding and 2-deoxyglucose (2-DOG) uptake data were analyzed for statistical significance using analysis of variance with the Bonferroni correction for multiple comparisons ($p < 0.05$).

RESULTS

Peptide Inhibition of Glucose Transport Activity—Indinavir, like all first generation HIV protease inhibitors, contains a core peptidomimetic structure with flanking hydrophobic moieties. We have shown previously that the peptide Z-HFFe, similar to indinavir, acts as a potent noncompetitive inhibitor of zero-trans GLUT4-mediated glucose transport but has little effect on GLUT1 transporter activity (11). Furthermore, a structurally related photoactivatable peptide, Z-HFF-Bpa-^{125}I-Tyr-*O*-ethyl ester, selectively labeled GLUT4 in rat adipocytes in an indinavir-inhibitable manner (11). To facilitate identification of the peptide binding site in GLUT4, HR-1, a modified form of Z-HFF-Bpa-^{125}I-Tyr-*O*-ethyl ester in which the radioactive label is replaced by two Ahx spacer linkages and a FLAG epitope, was created. To test the ability of HR-1, Z-HFFe, and CB to antagonize glucose transport in HEK293 cells stably overexpressing rat GLUT4, 2-DOG uptake was measured in the presence of these compounds and DMSO/ethanol (vehicles). Z-HFFe and CB but not HR-1 inhibited 2-DOG uptake compared with the vehicle controls (Fig. 1).

ATB-BMPA Labeling at the Endofacial Side of GLUT4—Extensive analysis of the kinetics of glucose transport has largely supported an alternating conformation model in which the glucose binding site cannot be simultaneously accessed from both sides of the plasma membrane (24, 25). Thus, the ability of indinavir to act as a noncompetitive inhibitor of zero-trans 2-DOG uptake (6) does not exclude the possibility that this drug acts as a competitive inhibitor of glucose binding at the endofacial/cytoplasmic transporter surface. We recently developed an ATB-BMPA photolabel binding assay that allows targeting of the glucose binding site of GLUTs from the cytoplasmic side (5). In this assay, LDMs prepared from 3T3-L1

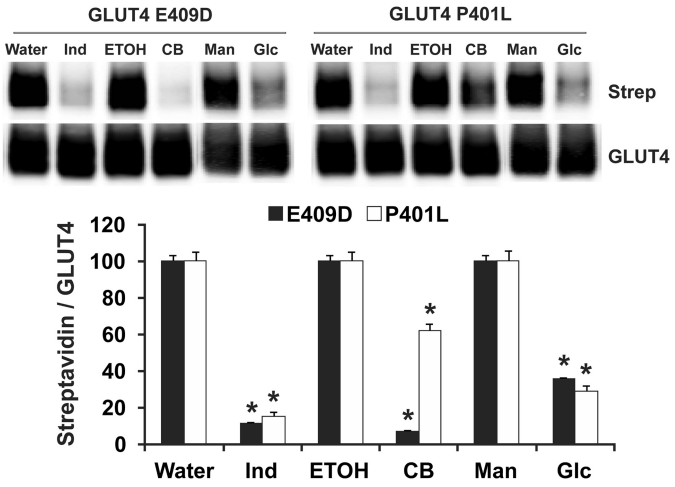

FIGURE 2. **ATB-BMPA photolabeling of LDMs isolated from HEK293 cells overexpressing two GLUT4 mutant transporters locked in an inward facing conformation.** For ATB-BMPA photolabeling, 200 μg of LDMs prepared from HEK293 cells overexpressing GLUT4 E409D and GLUT4 P401L was treated for 10 min at room temperature with 100 μM indinavir (*Ind*), 20 μM CB, 300 mM D-mannitol (*man*), 300 mM D-glucose (*Glc*), or the corresponding vehicle controls. Samples were then irradiated with biotinylated ATB-BMPA (50 μM final concentration) as described under "Experimental Procedures." Solubilized exogenously expressed GLUT4 mutant proteins were immunoprecipitated with anti-Myc antibodies. Immunoblots of the immunoprecipitates were analyzed for total GLUT4 mutant protein and biotinylated ATB-BMPA labeling using a GLUT4-specific antibody and fluorescently labeled streptavidin (*Strep*), respectively. For quantification of ATB-BMPA results, immunoblots were quantified using an Odyssey infrared imaging system. The fraction of transporter labeled by ATB-BMPA was determined from the ratio of streptavidin to GLUT4 transporter. Data normalized to vehicle controls represent the mean of four independent experiments. *Error bars* represent S.E. *, $p < 0.05$ *versus* vehicle control.

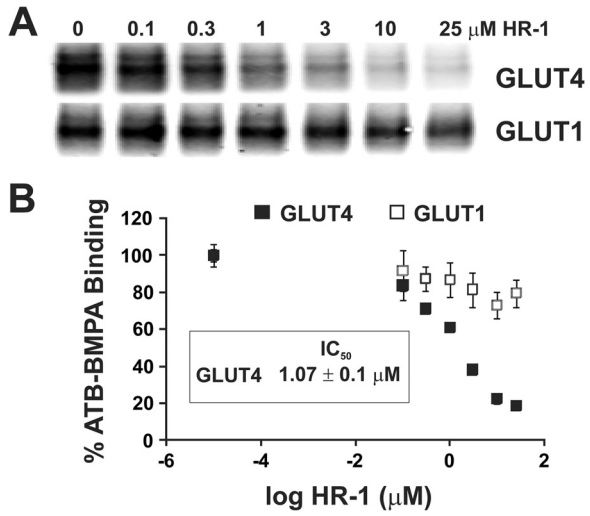

FIGURE 3. **Dose-response inhibition of ATB-BMPA photolabeling by HR-1.** *A*, ATB-BMPA photolabeling. DMSO (vehicle control) or HR-1 was added to 200 μg of LDMs prepared from 3T3-L1 adipocytes for 10 min at room temperature. Samples were then irradiated with biotinylated ATB-BMPA (50 μM final concentration) as described under "Experimental Procedures." Biotinylated proteins isolated from detergent-solubilized LDMs using a high capacity streptavidin-agarose resin were analyzed by immunoblot analysis using GLUT4 or GLUT1 antibodies. *B*, quantification of ATB-BMPA results. GLUT proteins were quantified using an Odyssey infrared imaging system. Data normalized to vehicle controls represent the mean of three independent experiments. *Error bars* represent S.E. Half maximal inhibition (IC_{50}) of ATB-BMPA binding to GLUT4 by HR-1 was determined using a nonlinear least square analysis (GraphPad Prism version 5.0).

adipocytes contain small intracellular vesicles of GLUT4 and GLUT1 in which the transporter orientation is inverted relative to that found in the PM. Immunoprecipitation of greater than 70% of the GLUT4-containing vesicles using an antibody that recognized the cytoplasmic GLUT4 carboxyl terminus confirmed the transporter membrane orientation. ATB-BMPA, however, has been reported to be an exofacial photolabel that presumably cannot label the transporter from the endofacial side (26). To address whether ATB-BMPA can in fact label glucose transporters from the cytoplasmic side, we carried out a photolabeling experiment using LDMs isolated from two different HEK293 cell lines, each overexpressing a GLUT4 mutant transporter containing a single amino acid substitution reported previously to lock the transporter in an inward facing conformation (27, 28). Specifically, when Glu-409 in GLUT4 was changed to Asp (28) and Pro-385 in GLUT1 was changed to a nonflexible amino acid (27), the resulting transporters possessed negligible transport activity and exofacial ATB-BMPA labeling but still had preserved CB binding (27, 28). In our study, robust ATB-BMPA labeling of GLUT4 E409D and GLUT4 P401L (corresponding to P385L in GLUT1) in LDMs was observed, and this labeling was inhibited by both indinavir and D-glucose (Fig. 2). Interestingly, CB strongly inhibits ATB-BMPA labeling of E409D but only weakly inhibits the labeling of P401L. These results clearly demonstrate that ATB-BMPA can label glucose transporters from the cytoplasmic side.

Inhibition of ATB-BMPA Photolabeling by HR-1—Previously we have shown that indinavir inhibits ATB-BMPA labeling of GLUT4 and GLUT1 with IC_{50} values of 20.7 and 178 μM, respectively (5). In addition, Scatchard binding analysis reveals that indinavir acts as a competitive inhibitor of ATB-BMPA, binding to GLUT4 in isolated LDMs with a K_i of 8.2 μM. If the Z-HFFe peptides similarly target GLUT4, these compounds would have to cross the PM to gain access to the transporter binding site. The inability of HR-1 to inhibit zero-trans 2-DOG uptake (Fig. 1) could, therefore, be due to the membrane-impermeant nature of HR-1 arising from the charged amino acid residues of the FLAG tag. To test for HR-1 binding to the endofacial transporter surface, we measured the effect of HR-1 on ATB-BMPA photolabeling of GLUT1 and GLUT4 in LDMs prepared from 3T3-L1 adipocytes. In comparison with indinavir, HR-1 is actually a more potent and specific inhibitor of ATB-BMPA labeling of GLUT4 with an IC_{50} of 1.07 $\pm$ 0.1 μM but was found to have almost no effect on the labeling of GLUT1 (Fig. 3).

Inhibition of HR-1 Labeling—HR-1 with its photolabel moiety Bpa was then used to label GLUT4 by substituting HR-1 for ATB-BMPA in the LDM labeling assay. Indinavir (IC_{50}, 17.4 $\pm$ 4 μM) and D-glucose inhibited the labeling of GLUT4 with HR-1 (Fig. 4). CB had only a minor effect on HR-1 labeling of GLUT4, suggesting that the amino acid residues involved in peptide and CB binding are distinct. GLUT1 was not specifically labeled with HR-1 because the band in the no UV control was just as intense as those found in the other lanes of the GLUT1 blot (Fig. 4).

Construction of GLUT1/GLUT4 Chimeras—To determine the molecular basis of the isoform-selective inhibition of ATB-BMPA labeling by indinavir and HR-1, a series of GLUT1/GLUT4 chimeric transporters were created and tested for PI

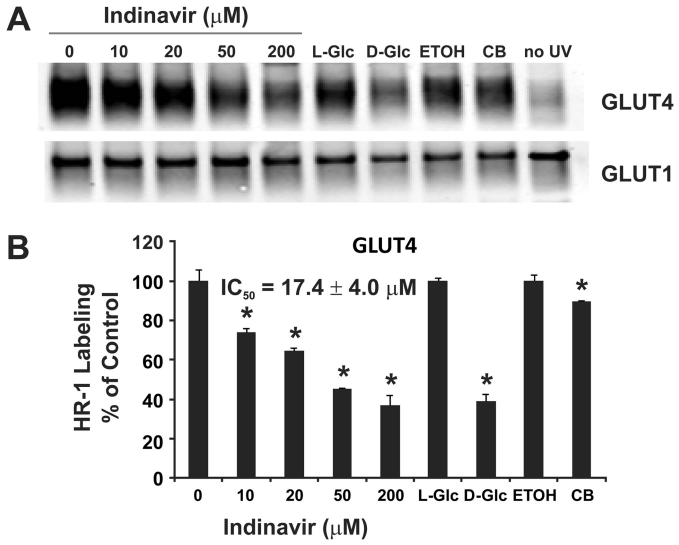

FIGURE 4. **Inhibition of HR-1 photolabeling by indinavir, D-glucose, and cytochalasin B.** *A*, HR-1 photolabeling. Indinavir, 500 mM L-glucose, 500 mM D-glucose, or 20 μM CB was added to 200 μg of LDMs prepared from 3T3-L1 adipocytes for 10 min at room temperature. Samples were then irradiated with HR-1 (2.5 μM final concentration) as described under "Experimental Procedures." FLAG-tagged proteins isolated from detergent-solubilized LDMs using α-FLAG affinity gel were analyzed by immunoblot analysis using GLUT4 or GLUT1 antibodies. *B*, quantification of HR-1 results. GLUT proteins were quantified using an Odyssey infrared imaging system. Data normalized to vehicle controls represent the mean of three independent experiments. *Error bars* represent S.E. Half maximal inhibition (IC_{50}) of HR-1 binding to GLUT4 by indinavir was determined using a nonlinear least square analysis (GraphPad Prism version 5.0). *, $p < 0.05$ *versus* vehicle control. *Glc*, glucose.

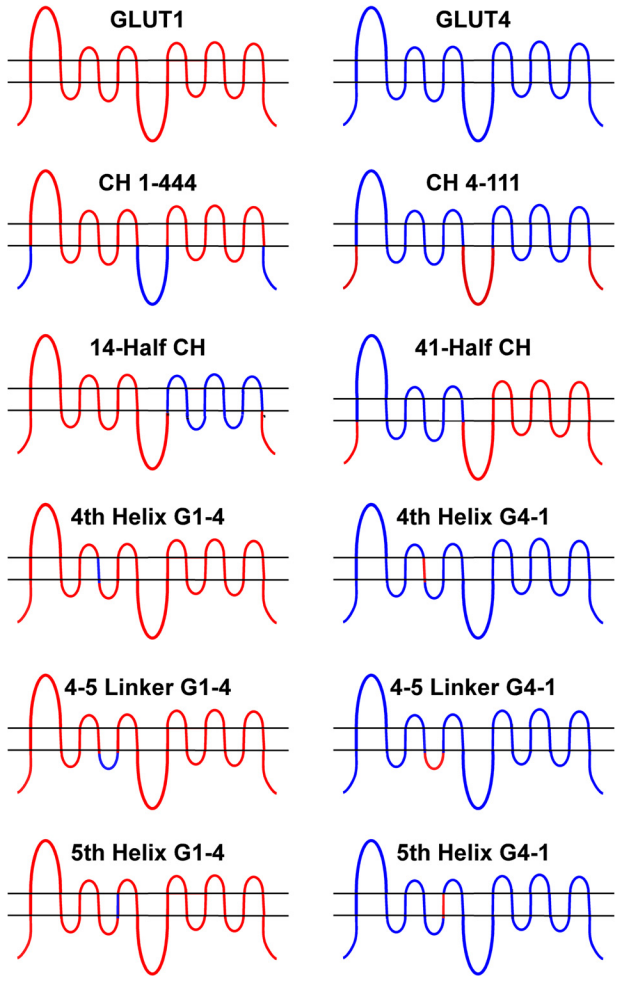

FIGURE 5. **Schematic topological diagrams of the GLUT1/GLUT4 chimeric transporters.** All chimeras contain a Myc tag in the first exofacial domain and six histidines at the end of the carboxyl terminus. GLUT1 sequence is depicted in *red*, and GLUT4 sequence is in *blue*. The nomenclature for CH 1-444 and CH 4-111 is as follows: the first number indicates whether the backbone amino acids are derived from GLUT1 or GLUT4, and the last three numbers signify the origin of the amino-terminal, large endofacial central loop, and carboxyl-terminal domains. The 14-half CH has GLUT1 sequence in TMs 1–6 and connecting loops with GLUT4 sequence in TMs 7–12 and connecting loops. The 41-half CH has the opposite configuration. Both half chimeras contain GLUT1 sequence in the amino-terminal, large central loop, and carboxyl-terminal domains. The three G1-4 chimeras entirely comprise GLUT1 sequence except for GLUT4 sequence in the fourth helix, fifth helix, or linker domain connecting the fourth and fifth helices, respectively. The three G4-1 chimeras have the opposite configuration.

and peptide binding. The chimeric transporters used are illustrated in Fig. 5 where GLUT1 sequence is shown in *red* and GLUT4 sequence is depicted in *blue*. Each transporter contains a Myc epitope in the first exofacial domain and a His_6 tag at the extreme carboxyl terminus. All chimeric transporters were stably expressed in HEK293 cells using retroviral expression to allow isolation of LDMs and assay of the ability of indinavir and HR-1 to alter ATB-BMPA photolabeling.

Inhibition of ATB-BMPA Photolabeling of GLUT1/GLUT4 Chimeric Transporters by Indinavir and HR-1—The first chimeric transporters analyzed were ones that exchanged the most divergent regions between GLUT1 and GLUT4, the cytoplasmic amino and carboxyl termini and the large endofacial loop. Chimera 1-444 contained the backbone of GLUT1 but the amino terminus, the large endofacial loop, and the carboxyl terminus of GLUT4. Chimera 4-111 had the opposite configuration. Wild type Myc-GLUT1-His and Myc-GLUT4-His transporters (subsequently, denoted as GLUT1 and GLUT4, respectively) were also expressed in HEK293 cells and used for comparison. Indinavir and HR-1 inhibited ATB-BMPA labeling of GLUT4 to a much higher degree relative to GLUT1 (Fig. 6). Inhibition by indinavir and HR-1 of ATB-BMPA labeling of CH 4-111 and CH 1-444 mimicked that observed for GLUT4 and GLUT1, respectively. CB inhibited ATB-BMPA labeling of all four constructs approximately the same. These data indicate that regions within the backbone of the transporter and not the amino terminus, the large central loop, or the carboxyl terminus are responsible for the isoform-selective inhibition of ATB-BMPA labeling by indinavir and HR-1.

The next two chimeras analyzed contained approximately half of each transporter isoform sequence at either the amino or carboxyl terminal domains. The 14-half chimera had the amino-terminal half of GLUT1 and the carboxyl-terminal half of GLUT4, and the 41-half chimera had the opposite configuration. Both chimeras contained GLUT1 sequence in the cytoplasmic amino terminus, the large endofacial loop, and the cytoplasmic carboxyl terminus. ATB-BMPA labeling inhibition by indinavir and HR-1 of the 14-half CH and the 41-half CH almost exactly mirrored the GLUT1 and GLUT4 results, respectively (Fig. 7). CB strongly inhibited ATB-BMPA labeling of the two half chimeras and the two wild type transporters to the same extent. These results indicate that the amino-terminal half of the transporter, excluding the cytoplasmic amino termi-

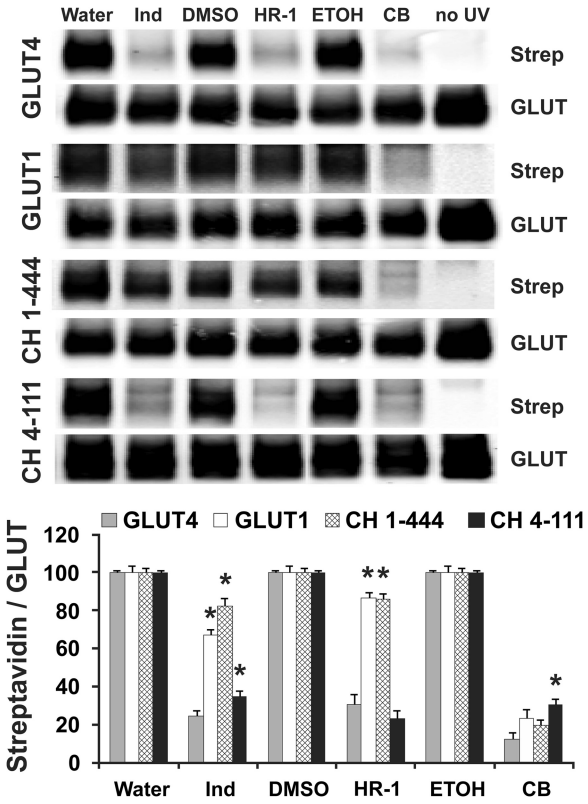

FIGURE 6. **The GLUT isoform specificity of inhibition of ATB-BMPA labeling by indinavir and HR-1 is not dependent on the large endofacial central loop or the amino and carboxyl termini.** For ATB-BMPA photolabeling, 200 μg of LDMs prepared from HEK293 cells overexpressing GLUT4, GLUT1, CH 1-444, and CH 4-111 was treated for 10 min at room temperature with 100 μM indinavir (*Ind*), 5 μM HR-1, 20 μM CB, or the corresponding vehicle controls. Samples were then irradiated with biotinylated ATB-BMPA (50 μM final concentration) as described under "Experimental Procedures." Solubilized exogenously expressed GLUT proteins were immunoprecipitated with anti-Myc antibodies. Immunoblots of the immunoprecipitates were analyzed for total GLUT protein and biotinylated ATB-BMPA labeling using a GLUT-specific antibody and fluorescently labeled streptavidin (*Strep*), respectively. For quantification of ATB-BMPA results, immunoblots were quantified using an Odyssey infrared imaging system. The fraction of transporter labeled by ATB-BMPA was determined from the ratio of streptavidin to GLUT transporter. Data normalized to vehicle controls represent the mean of four independent experiments. *Error bars* represent S.E. *, $p < 0.05$ *versus* GLUT4 control.

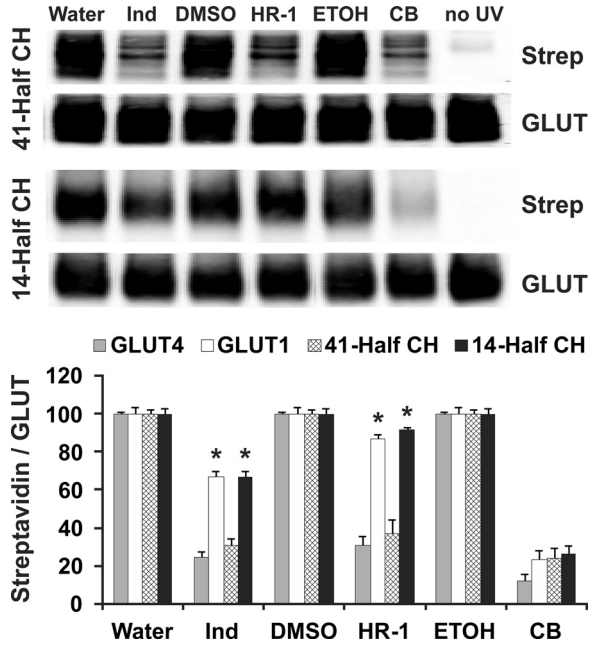

FIGURE 7. **The amino-terminal half of GLUT4 is necessary and sufficient for the inhibition of ATB-BMPA labeling by indinavir and HR-1.** 200 μg of LDMs prepared from HEK293 cells overexpressing 14-half CH and 41-half CH was treated for 10 min at room temperature with 100 μM indinavir (*Ind*), 5 μM HR-1, 20 μM CB, or the corresponding vehicle controls. ATB-BMPA photolabeling and subsequent analysis were carried out as described in Fig. 6 legend. GLUT4 and GLUT1 results are shown for comparison. *Error bars* represent S.E. *, $p < 0.05$ *versus* GLUT4 control. *Strep*, streptavidin.

nus and the large central loop, is responsible for the isoform-selective inhibition by indinavir and HR-1. This region of the transporter is necessary and sufficient for the observed selectivity. These results are also consistent with our earlier observation that the amino acid side chains necessary for HR-1 and CB binding are distinct. Trp-388 and Trp-412 (GLUT1 amino acid numbering), which are important for CB binding, are both located within the carboxyl-terminal half of the transporter (29).

As has been reported previously (30) and confirmed in our current study (Fig. 2), D-glucose inhibits its transporter labeling with ATB-BMPA. This together with consideration of the structure of this photolabel led us to hypothesize that the binding site in our LDM assay resides within the putative aqueous pore of the transporter. We excluded helices 3 and 6 as important in isoform-selective inhibition because both the recently reported crystal structure of the *Escherichia coli* xylose transporter (XylE) (31) and previously published cysteine-scanning mutagenesis data from GLUT1 (32) indicate that these two helices are located outside the aqueous channel. Therefore, we elected to focus on further investigation of TM helices 4 and 5 together with the endofacial linker domain between these two TM regions. Three GLUT4 chimeras (G4-1) were constructed in which amino acid residues in the fourth helix, the 4-5 linker domain, and the fifth helix were changed to those found in GLUT1. Conversely, three GLUT1 chimeras (G1-4) were constructed in which amino acid residues in the same three regions were changed to GLUT4. ATB-BMPA labeling of the G4-1 chimeras (Fig. 8*A*) demonstrates that changing the fourth helix, the 4-5 linker, or the fifth helix to GLUT1 had no effect on the inhibition by indinavir when compared with the GLUT4 results. Likewise, changing amino acids found in the fourth helix and the 4-5 linker of GLUT4 to those found in GLUT1 also had no effect on HR-1 inhibition when compared with GLUT4. However, changing amino acid residues in the fifth helix of GLUT4 to GLUT1 resulted in a loss of HR-1 inhibition of ATB-BMPA labeling similar to GLUT1. CB strongly inhibited ATB-BMPA binding in all three G4-1 chimeras to the same extent. Conversely, changing amino acids in the fourth helix and the 4-5 linker domain in GLUT1 to those in GLUT4 did not affect the inhibition of ATB-BMPA labeling by indinavir when compared with the results for GLUT1 (Fig. 8*B*). However, when the fifth helix of GLUT1 was changed to GLUT4, the inhibition by indinavir was in between the inhibition observed for GLUT1 and GLUT4. Inhibition by HR-1 for all three G1-4 chimeras mimicked GLUT1. As expected, CB strongly inhibited all three G1-4 chimeras to the same extent.

Based on the ATB-BMPA binding data, TM5 contains amino acid residues that contribute to the isoform-selective inhibition

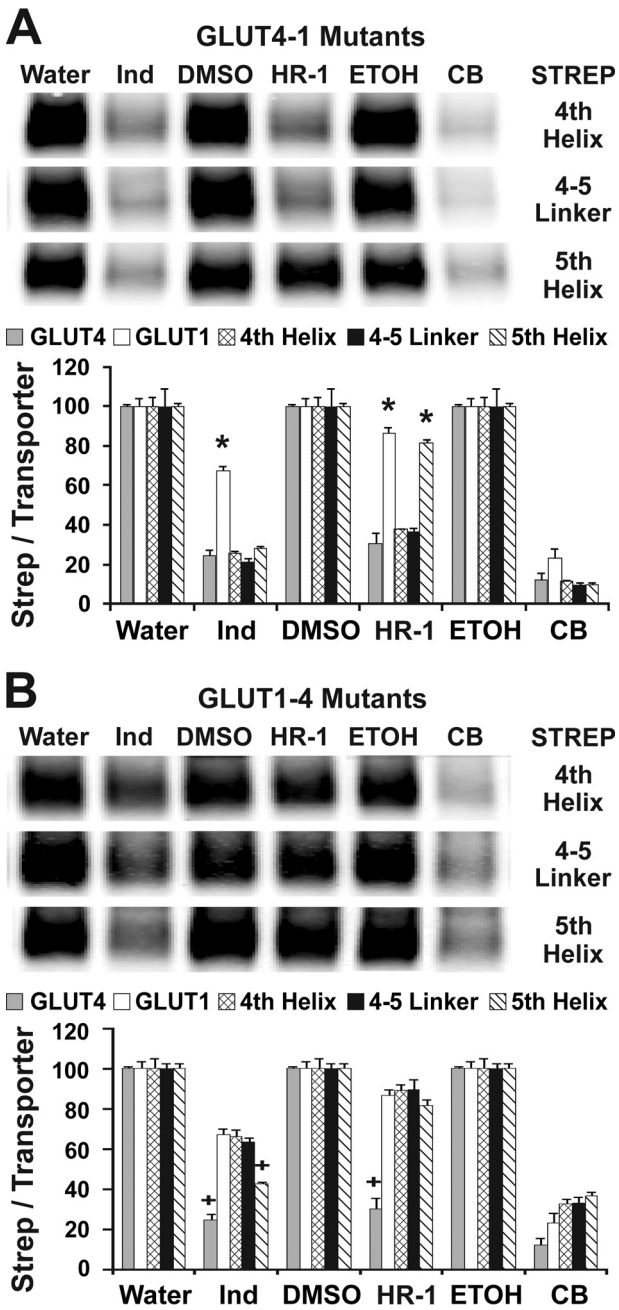

FIGURE 8. **The fifth helix of GLUT4 is critically important in the inhibition of ATB-BMPA labeling by indinavir and HR-1.** *A*, ATB-BMPA photolabeling of GLUT4-1 mutants. The three G4-1 chimeras entirely comprise GLUT4 sequence except for GLUT1 sequence in the fourth helix, fifth helix, or linker domain connecting the fourth and fifth helices. 200 μg of LDMs prepared from HEK293 cells overexpressing each of the three GLUT4-1 mutants was treated for 10 min at room temperature with 100 μM indinavir (*Ind*), 5 μM HR-1, 20 μM CB, or the corresponding vehicle controls. ATB-BMPA photolabeling and subsequent analysis were carried out as described in Fig. 6 legend. GLUT4 and GLUT1 results are shown for comparison. *, $p < 0.05$ *versus* GLUT4 control. *B*, ATB-BMPA photolabeling of GLUT1-4 mutants. The three G1-4 chimeras entirely comprise GLUT1 sequence except for GLUT4 sequence in the fourth helix, fifth helix, or linker domain connecting the fourth and fifth helices. ATB-BMPA labeling and quantification were as described in *A*. +, $p < 0.05$ *versus* GLUT1 control. *Error bars* represent S.E. *Strep*, streptavidin.

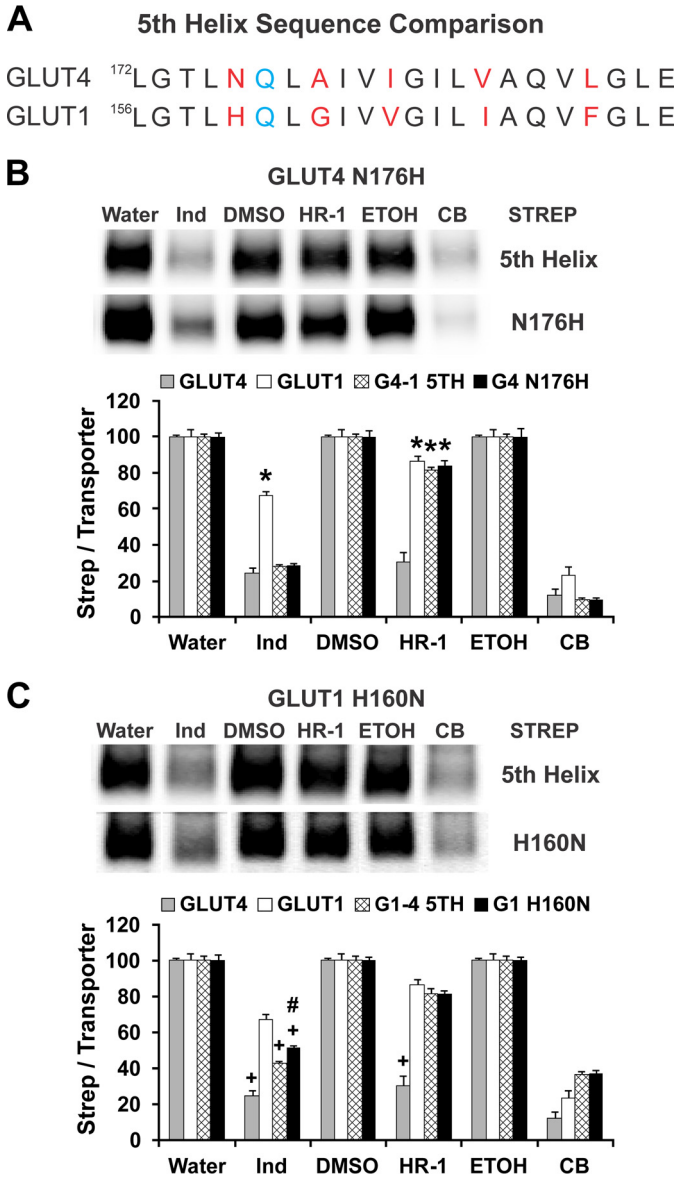

FIGURE 9. **Transposition of histidine and asparagine in TM5 of GLUTs 1 and 4 influences the ability of indinavir and HR-1 to inhibit ATB-BMPA binding.** *A*, fifth helix sequence comparison between rat GLUT1 and rat GLUT4. Unique amino acids are shown in *red*. Glutamine, shown in *blue*, participates in glucose binding. *B*, ATB-BMPA photolabeling of GLUT4 N176H. 200 μg of LDMs prepared from HEK293 cells overexpressing GLUT4 N176H was treated for 10 min at room temperature with 100 μM indinavir (*Ind*), 5 μM HR-1, 20 μM CB, or the corresponding vehicle controls. ATB-BMPA photolabeling and subsequent analysis were carried out as described in Fig. 6 legend. GLUT4, GLUT1, and GLUT4-1 fifth helix results are shown for comparison. *, $p < 0.05$ *versus* GLUT4 control. *C*, ATB-BMPA photolabeling of GLUT1 H160N. ATB-BMPA labeling and quantification were as described in *A*. GLUT4, GLUT1, and GLUT1-4 fifth helix results are shown for comparison. +, $p < 0.05$ *versus* GLUT1 control; #, $p < 0.05$ *versus* GLUT1-4 fifth helix. *Error bars* represent S.E. *Strep*, streptavidin.

by indinavir and HR-1. The most dramatic amino acid change in the fifth helix between GLUT1 and GLUT4 is His-160 in GLUT1 that corresponds to Asn-176 in GLUT4 (Fig. 9*A*). Histidine is a basic amino acid with a bulky imidazole ring. Asparagine is a neutral amino acid with a carboxamide side chain. Interestingly, both amino acids are immediately adjacent to a glutamine that is part of the glucose binding site (33). Consequently, GLUT4 N176H and GLUT1 H160N were made to test the effect of exchanging these two amino acids in terms of the inhibition of ATB-BMPA labeling by indinavir and HR-1. Changing Asn-176 to His in GLUT4 resulted in the same inhibition of ATB-BMPA labeling by indinavir and HR-1 as was

observed when changing the whole fifth helix in GLUT4 to GLUT1, chimera GLUT4-1 5th helix (Fig. 9*B*). Conversely, inhibition of ATB-BMPA labeling by indinavir and HR-1 of GLUT1 H160N was almost identical to that seen using the GLUT1-4 5th helix chimera (Fig. 9*C*). The slight difference in the indinavir inhibition between GLUT1 H160N and the GLUT1-4 5th helix chimera suggests there may be additional amino acids in the fifth helix of GLUT1 other than His-160 that may also contribute to isoform-selective inhibition. As expected, CB strongly inhibited ATB-BMPA labeling of GLUT4 N176H and GLUT1 H160N. Overall, these results indicate that His-160 in GLUT1 and Asn-176 in GLUT4 are the major residues in the fifth helix that influence the ability of indinavir and HR-1 to inhibit ATB-BMPA labeling.

In addition to the fifth helix, the binding data indicate that there are other residues in the amino-terminal half of the transporter that are important in the isoform-selective inhibition by indinavir and HR-1. XylE and the 14 GLUT transporters are members of the major facilitator superfamily and share 20–29% sequence identity including all of the GLUT signature motifs (31). The helical packing is predicted to be very similar among these transporters. Based on the x-ray crystallographic structure of XylE, the carboxyl-terminal half of TM1 is situated between TM5 and TM4 in the glucose permeation pathway (31). Amino acid residues in the carboxyl-terminal half of TM1 for GLUT1 and GLUT4 are identical except for Thr-30 in GLUT1 that corresponds to Ile-42 in GLUT4 (Fig. 10*A*). This represents a nonconservative amino acid change from a nucleophilic residue, Thr, to a hydrophobic residue, Ile. Consequently, we tested whether the transposition of Thr/Ile in TM1 had an effect in terms of the inhibition of ATB-BMPA labeling by indinavir and HR-1 either alone or in combination with His/Asn in TM5. Changing Ile-42 to Thr in GLUT4 either alone or in combination with N176H did not significantly affect indinavir inhibition of ATB-BMPA labeling (Fig 10*B*). HR-1 inhibition of ATB-BMPA labeling of GLUT4 I42T was decreased compared with that observed with GLUT4 and identical to that of GLUT1 in the GLUT4 I42T/N176H double mutation. CB strongly inhibited ATB-BMPA labeling of both GLUT4 I42T and GLUT4 I42T/N176H but less than that observed for GLUT4. Changing Thr-30 to Ile in GLUT1 increased the indinavir inhibition of ATB-BMPA labeling compared with GLUT1 to a higher degree than was observed when His-160 was changed to Asn in GLUT1 (Fig. 10*C*). In conjunction with H160N mutation, changing Thr-30 to Ile in GLUT1 had an additive effect in terms of the inhibition of ATB-BMPA labeling by indinavir to a level indistinguishable with that seen for GLUT4. The T30I mutation in GLUT1 alone or in combination with H160N had little effect on HR-1 inhibition of ATB-BMPA labeling. CB inhibition of ATB-BMPA labeling of both GLUT1 T30I and GLUT1 T30I/H160N was statistically the same as GLUT1.

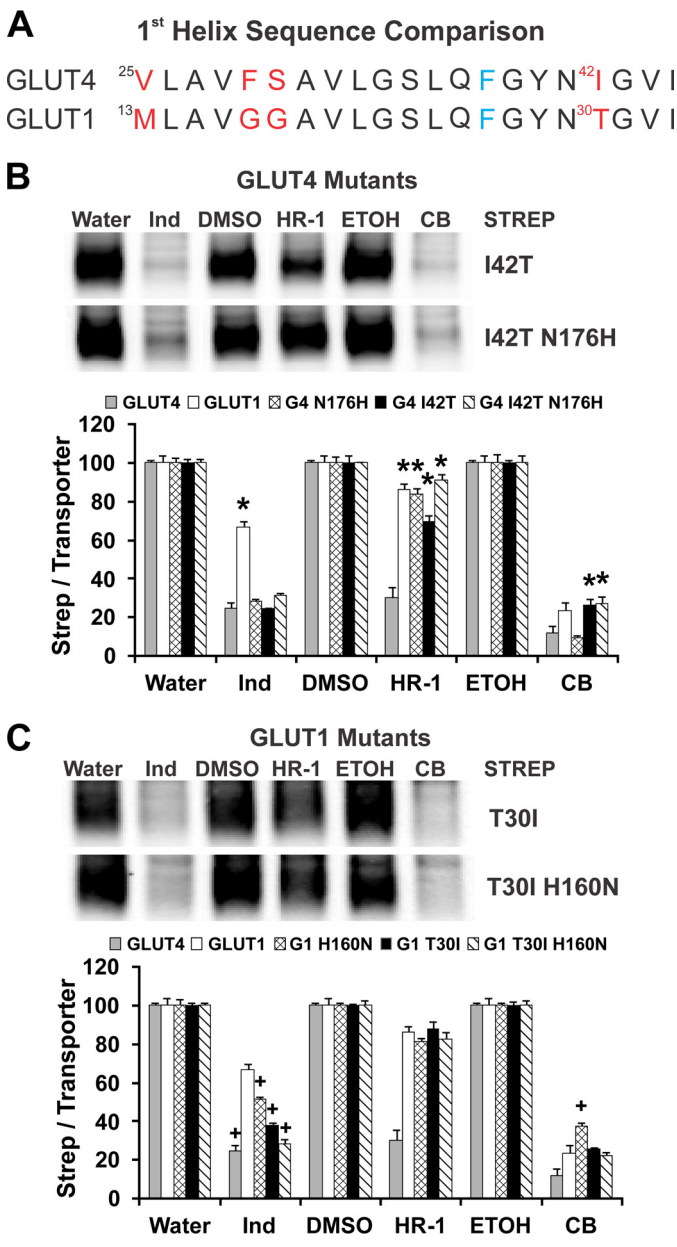

FIGURE 10. **Transposition of threonine and isoleucine in TM1 of GLUT1s 1 and 4 influences the ability of indinavir and HR-1 to inhibit ATB-BMPA binding.** *A*, first helix sequence comparison between rat GLUT1 and rat GLUT4. Unique amino acids are shown in *red*. Phenylalanine, shown in *blue*, participates in the delimitation of the glucose binding site. *B*, ATB-BMPA photolabeling of GLUT4 I42T and GLUT4 I42T/N176H. 200 μg LDMs prepared from HEK293 cells overexpressing GLUT4 I42T and GLUT4 I42T/N176H was treated for 10 min at room temperature with 100 μM indinavir (*Ind*), 5 μM HR-1, 20 μM CB, or the corresponding vehicle controls. ATB-BMPA photolabeling and subsequent analysis were carried out as described in Fig. 6 legend. GLUT4, GLUT1, and GLUT4 N176H results are shown for comparison. *, $p < 0.05$ *versus* GLUT4 control. *C*, ATB-BMPA photolabeling of GLUT1 T30I and GLUT1 T30I/H160N. ATB-BMPA labeling and quantification were as described in *A*. GLUT4, GLUT1, and GLUT1 H160N results are shown for comparison. +, $p < 0.05$ *versus* GLUT1 control. *Error bars* represent S.E.

Inhibition of Chimeric Transporter Activity by Indinavir and Z-HFFe—The functional integrity of the chimeric transporters was assessed by measuring 2-DOG uptake. Initial uptake experiments were conducted in untransfected 293 cells and 293 cells expressing GLUT4, GLUT1, and the two inactive GLUT4 mutants, E409D and P401L (Fig 11*A*). 2-DOG uptake in cells expressing either E409D or P401L was only slightly higher than that of untransfected 293 cells. The difference in uptake is due to residual activity of the mutant transporters and/or a retrovirus-induced increase in endogenous transporter activity. Indinavir inhibited uptake ~30% in each of these three cell lines. 2-DOG uptake in cells expressing GLUT4 or GLUT1 was between 2.5- and 3-fold higher than that of untransfected cells

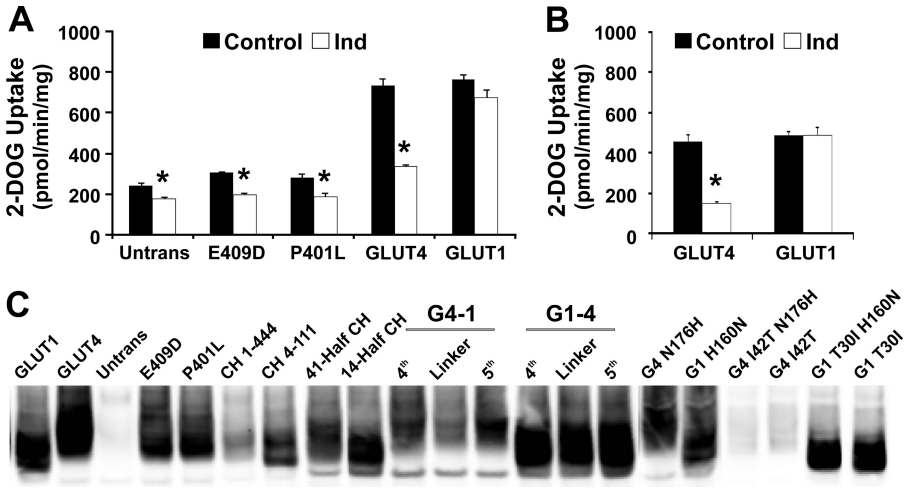

FIGURE 11. **2-Deoxyglucose uptake of GLUT4 and GLUT1 in 293 cells.** *A*, 2-DOG uptake. Indinavir (*Ind*) (50 μM) was added 6 min prior to glucose uptake in untransfected (*Untrans*) 293 cells and 293 cells expressing GLUT4, GLUT1, and the GLUT4 dead mutants E409D and P401L. 2-Deoxy[^{3}H]glucose uptake was measured at 37 °C for 6 min as described under "Experimental Procedures." Data shown are mean uptakes relative to control ($n = 3$). *Error bars* represent S.E. *, $p < 0.05$ *versus* vehicle control. *B*, specific GLUT4 and GLUT1 uptake. Uptake from the GLUT4 P401L cells (control and indinavir) was subtracted from the corresponding GLUT4 and GLUT1 data shown in *A*. *C*, relative expression of the chimeric transporters. Whole cell lysates (15 μg) from untransfected 293 cells and 293 cells expressing exogenous wild type and chimeric transporters were analyzed by immunoblot analysis using a Myc-specific antibody.

or cells expressing E409D or P401L. Indinavir inhibited 2-DOG uptake 55% in GLUT4 cells and had little effect in GLUT1 cells. To allow assessment of the specific effect of indinavir on exogenously expressed transporters, 2-DOG uptake values of the P401L cell line were used to approximate the contribution of the endogenous transporters and any virus-induced effects. Changing proline to leucine is a dramatic change of an important amino acid residue that is likely to totally abolish transport activity. The transport activity of the exogenously expressed protein after subtraction of 2-DOG uptake values of the P401L GLUT4-expressing cells (control and indinavir) are shown in Fig 11*B*. Both GLUT4 and GLUT1 were functionally active in terms of 2-DOG uptake. Indinavir inhibited GLUT4 transporter activity ~65–70% but had essentially no effect on GLUT1.

Uptake of 2-DOG was then assessed in 293 cells expressing each of the different GLUT1/GLUT4 chimeric transporters generated. Chimeric uptake after subtracting the P401L uptake values are shown in Tables 1 and 2. The levels of expression of CH 1-444, GLUT4 I42T, and GLUT4 I42T/N176H were the lowest of the exogenous transporters (Fig 11*C*). Although the levels of expression of these particular transporters were high enough for the LDM ATB-BMPA binding assay, the expression at the PM was too low for activity measurements. Sorting cells expressing these transporters using a Myc antibody that recognized the Myc epitope inserted into the first exofacial loop of the transporters still failed to increase 2-DOG uptake above background. In addition to expression, targeting of the exogenous transporter may influence uptake. We have shown previously in 3T3-L1 adipocytes that indinavir does not acutely alter insulin signaling or cell surface transporter levels (4). HEK293 cells are not responsive to acute insulin in terms of 2-DOG uptake[3]; therefore, targeting effects due to brief exposure (6 min) to indinavir seem unlikely. It is possible, however, that these particular transporters are specifically targeted after synthesis to an intracellular compartment that fails to recycle with the PM, resulting in negligible uptake above background. Nevertheless, transport activity for all other transporters was significantly above the P401L control, demonstrating that the other chimeric GLUTs were functionally active. In terms of indinavir inhibition, the normalized 2-DOG uptake results were very similar to the normalized ATB-BMPA binding results (Table 1). Indinavir inhibition of CH 4-111, 41-half CH, the three G4-1 chimeric transporters, and GLUT4 N176H was very similar to that observed for GLUT4, and the indinavir inhibition of 14-half CH, G1-4 4th helix, and G1-4 4-5 linker transporters was very similar to that observed for GLUT1 for both 2-DOG uptake and ATB-BMPA binding. The two exceptions in which the uptake results differed from the binding results were for G1-4 5th helix and GLUT1 H160N. Indinavir inhibition of ATB-BMPA labeling of both of these transporters was in between that observed for GLUT1 and GLUT4, whereas the indinavir inhibition of 2-DOG uptake was similar to that of GLUT1. Uptake and binding results in terms of indinavir inhibition were also very similar for GLUT1 T30I and GLUT1 T30I/H160N. Most importantly, changing Thr-30 to Ile and His-160 to Asn in GLUT1 completely transforms GLUT1 into GLUT4 in terms of indinavir inhibition of 2-DOG uptake and ATB-BMPA.

HR-1 could not be used to inhibit 2-DOG uptake because our earlier results suggested that HR-1 cannot cross the PM (Fig. 1). Therefore, we used the membrane-permeable peptide Z-HFFe. The inhibition of chimeric uptake by Z-HFFe after subtracting the P401L uptake values are shown in Table 2. In all cases, the inhibition of 2-DOG uptake by Z-HFFe was very similar in terms of percentage of control and isoform selectivity to the indinavir uptake results. Inhibition of 2-DOG uptake by Z-HFFe was also very similar to the HR-1 inhibition of ATB-BMPA binding for most of the chimeric transporters. The exceptions were G4-1 5th helix and GLUT4 N176H in which

[3] R. C. Hresko, T. E. Kraft, A. Tzekov, S. A. Wildman, and P. W. Hruz, unpublished observation.

TABLE 1

Comparison of indinavir inhibition of 2-DOG uptake and ATB-BMPA binding

2-DOG uptake and ATB-BMPA binding were measured as described under "Experimental Procedures." Results shown in bold face text highlight key differences in labeling and transport activity between wild-type and chimeric transporters.

Transporter[a]	2-DOG uptake[b] Control	2-DOG uptake[b] Indinavir	2-DOG uptake[b] indinavir inhibition	ATB-BMPA binding indinavir inhibition
	pmol/min/mg		*% of control*	*% of control*
GLUT4	455 ± 34	149 ± 8	**33 ± 2**	**25 ± 3**
CH 4-111	91 ± 13	7 ± 11	8 ± 11[c]	35 ± 3[c]
41-half CH	185 ± 15	46 ± 12	25 ± 7	31 ± 4
G4-1 4th helix	348 ± 10	113 ± 16	32 ± 5	25 ± 2
G4-1 4-5 linker	281 ± 45	41 ± 12	15 ± 4[c]	21 ± 2
G4-1 5th helix	362 ± 31	97 ± 4	27 ± 1	28 ± 1
GLUT4 N176H	484 ± 23	140 ± 13	29 ± 3	29 ± 1
G4 I42T	ND	ND	ND	25 ± 0.3
G4 I42T/N176H	ND	ND	ND	32 ± 1
GLUT1	555 ± 25	529 ± 39	**95 ± 7**	**67 ± 3**
CH 1-444	ND	ND	ND	83 ± 4[d]
14-half CH	123 ± 26	110 ± 8	89 ± 7	67 ± 3
G1-4 4th helix	805 ± 49	746 ± 46	93 ± 6	66 ± 4
G1-4 4-5 linker	1035 ± 40	805 ± 66	78 ± 6	64 ± 2
G1-4 5th helix	805 ± 37	656 ± 43	82 ± 5	43 ± 1[d]
GLUT1 H160N	794 ± 16	669 ± 7	84 ± 1	52 ± 3[d]
G1 T30I	1176 ± 108	339 ± 27	29 ± 2[d]	38 ± 1[d]
G1 T30I/H160N	1636 ± 169	358 ± 66	**22 ± 4**[d]	**28 ± 2**[d]

[a] Schematic diagrams of chimeric transporters are shown in Fig. 5.
[b] GLUT4 P401L uptake (control, 209 pmol/min/mg; indinavir, 147 pmol/min/mg) was subtracted. Data shown are mean uptakes ±S.E. ($n = 4$). ND, not detectable above GLUT4 P401L uptake.
[c] $p < 0.05$ *versus* GLUT4 percentage of control.
[d] $p < 0.05$ *versus* GLUT1 percentage of control as determined by analysis of variance test with a Bonferroni correction.

TABLE 2

Comparison of Z-HFFe inhibition of 2-DOG uptake and HR-1 inhibition of ATB-BMPA binding

2-DOG uptake and ATB-BMPA binding were measured as described under "Experimental Procedures." Results shown in bold face text highlight key differences in labeling and transport activity between wild-type and chimeric transporters.

Transporter[a]	2-DOG uptake[b] Control	2-DOG uptake[b] Z-HFFe	2-DOG uptake[b] Z-HFFe inhibition	ATB-BMPA binding HR-1 inhibition
	pmol/min/mg		*% of control*	*% of control*
GLUT4	575 ± 20	141 ± 14	**25 ± 3**	**30 ± 5**
CH 4-111	201 ± 23	27 ± 3	13 ± 2[c]	23 ± 4
41-half CH	232 ± 20	54 ± 5	23 ± 2	37 ± 7
G4-1 4th helix	332 ± 35	59 ± 11	18 ± 3	38 ± 0.3
G4-1 4-5 linker	242 ± 25	36 ± 10	15 ± 4	37 ± 2
G4-1 5th helix	425 ± 34	116 ± 15	27 ± 3	81 ± 2[c]
GLUT4 N176H	441 ± 28	100 ± 6	23 ± 1	84 ± 4[c]
G4 I42T	ND	ND	ND	70 ± 3[c]
G4 I42T/N176H	ND	ND	ND	91 ± 3[c]
GLUT1	672 ± 29	522 ± 24	**78 ± 4**	**87 ± 3**
CH 1-444	ND	ND	ND	86 ± 4
14-half CH	169 ± 11	113 ± 9	67 ± 5	92 ± 2
G1-4 4th helix	477 ± 13	418 ± 11	88 ± 2	89 ± 3
G1-4 4-5 linker	661 ± 27	500 ± 24	76 ± 4	90 ± 5
G1-4 5th helix	531 ± 20	429 ± 29	81 ± 6	82 ± 3
GLUT1 H160N	808 ± 7	548 ± 34	68 ± 4	82 ± 1
G1 T30I	946 ± 70	348 ± 7	37 ± 1[d]	88 ± 4
G1 T30I/H160N	1365 ± 28	367 ± 79	**27 ± 7**[d]	**83 ± 4**

[a] Schematic diagrams of chimeric transporters are shown in Fig. 5.
[b] GLUT4 P401L uptake (control, 242 pmol/min/mg; Z-HFFe, 122 pmol/min/mg) was subtracted. Data shown are mean uptakes ±S.E. ($n = 4$). ND, not detectable above GLUT4 P401L uptake.
[c] $p < 0.05$ *versus* GLUT4 percentage of control.
[d] $p < 0.05$ *versus* GLUT1 percentage of control as determined by analysis of variance test with a Bonferroni correction.

Z-HFFe inhibition of 2-DOG uptake was similar to that observed with GLUT4, but HR-1 inhibition of ATB-BMPA binding was similar to that of GLUT1. In addition, inhibition of uptake by Z-HFFe was greater than the inhibition of ATB-BMPA binding by HR-1 for both GLUT1 T30I and GLUT1 T30I/H160N. Similar to the indinavir inhibition of 2-DOG uptake, changing Thr-30 to Ile and His-160 to Asn in GLUT1 completely transforms GLUT1 into GLUT4 in terms of inhibition of 2-DOG uptake by Z-HFFe.

Homology Modeling of the PI Binding Site in GLUT4—The above ATB-BMPA binding and 2-DOG uptake studies provided a basis to investigate in more detail amino acid residues within the aqueous glucose permeation pathway of GLUT4 that contribute to indinavir binding. Using the known x-ray structures of XylE (34) and *Staphylococcus epidermidis* glucose/H^+ symporter (35) and established modeling algorithms, we generated a homology model of GLUT4 in an inward facing conformation and performed *in silico* binding analysis of indinavir in multiple orientations. GLUT4 Asn-176 consistently showed ability to interact with indinavir via hydrogen bonding (Fig. 12). Whereas GLUT4 Ile-42 did not appear to contribute directly to PI binding, it did delineate the indinavir binding pocket.

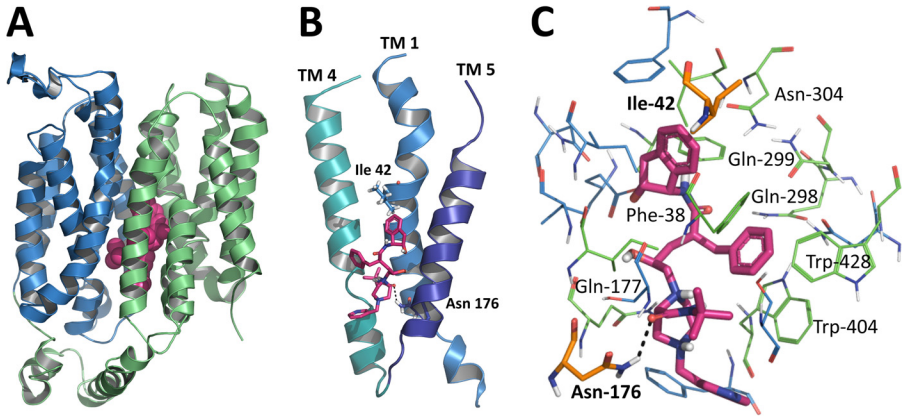

FIGURE 12. **Indinavir docked within the glucose permeation channel of the GLUT4 homology model.** *A*, indinavir (*pink*) within the glucose permeation pathway of GLUT4 in its inward open conformation. The amino-terminal half of GLUT4 is colored *blue*, and the carboxyl-terminal half is *green*. *B*, close-up of the three transmembrane helices 1, 4, and 5 that were studied by mutational analysis and indinavir. Residues Ile-42 and Asn-176 that were identified as being important for isoform selectivity are depicted in *stick* representation. *C*, putative indinavir binding site. Residues important for glucose binding are colored *green*, residues identified as being important for isoform selectivity are colored *orange*, and additional residues lining the indinavir binding site are colored *blue*.

Although this model supports the involvement of TM helices 1 and 5 in the binding of indinavir to GLUT4 within the glucose permeation pathway, several additional amino acid residues within the boundaries of this aqueous channel, some of which are reportedly involved in glucose binding, are also seen as candidates for potentially influencing drug binding. Thus, despite the limitations of modeling a system that undergoes significant conformation changes, this model is consistent with the current photolabeling data and provides novel insight into the molecular basis for the selective ability of indinavir to influence the intrinsic activity of GLUT4.

DISCUSSION

Identification of the structural features in GLUTs 1 and 4 that confer resistance and susceptibility to drug inhibition holds great promise for developing pharmacologic strategies to selectively target these glucose transporter isoforms. The current data identify a structural basis for the observed selectivity of indinavir to inhibit GLUT4 over GLUT1. Specifically, two amino acid residues in GLUT1 (Thr-30 and His-160) appear to hinder access to a binding pocket located within the central aqueous glucose permeation pathway. The observed differences in the affinities of indinavir and HR-1 to GLUT4 over GLUT1 are consistent with the results of Hellwig and Joost (36) who previously demonstrated similar differences in the binding of inhibitory ligands CB, forskolin, dipyridamole, and isobutylmethylxanthine for GLUTs 1, 2, and 4. These authors speculated that observed differences arise from the interaction of these compounds at distinct protein binding sites. As ATB-BMPA is a bismannose derivative that competes with glucose for binding presumably within the aqueous channel of the transporter, it is not surprising that the TM region is important in isoform-selective inhibition. Identification of aqueous accessible amino acid residues that presumably line this channel has been made through the use of cysteine-scanning mutagenesis of GLUT1 heterologously expressed in *Xenopus* oocytes (32). In those experiments, the engineered cysteine residues were labeled from the exofacial side of the plasma membrane. Labeling of the transporter in an inverted orientation relative to the plasma membrane provides support for the accessibility of these domains from the cytosolic surface of the transporter. Photolabeling of GLUT1 with the transportable diazirine glucose analog 3-deoxy-3,3-azi-D-glucopyranose identified labeled amino acids within both amino- and carboxyl-terminal transporter domains. Interestingly, this included both TM segments 4 and 5 (37).

Comparison of ATB-BMPA binding and 2-DOG uptake data in our current study demonstrates that changing Thr-30 to Ile and His-160 to Asn in GLUT1 is sufficient to transform GLUT1 into GLUT4 in terms of susceptibility to PI-mediated inhibition. Like GLUT1, GLUT3 has a Thr residue in the corresponding location in TM1, but like GLUT4, it has an Asn residue in the corresponding location in TM5. Interestingly, we have observed indinavir inhibition of ATB-BMPA labeling of GLUT3 in between that observed for GLUT4 and GLUT1 (data not shown). Changing PI susceptibility of GLUT1 into that of GLUT4 was easier than the converse experiment. The observed effects of changing Thr-30 to Ile and His-160 to Asn in GLUT1 can be caused either by direct disruption of the PI binding site or modulation of access to this site. If these mutations affected the binding site directly, then performing the converse experiment (*i.e.* changing Ile-42 to Thr and Asn-176 to His in GLUT4) should result in a dramatic decrease in the inhibition of ATB-BMPA labeling by indinavir. However, there was very little difference in the indinavir susceptibility of ATB-BMPA labeling between GLUT4 and GLUT4 I42T/N176H, suggesting that access to the PI binding site is altered with indinavir having greater access to the PI binding site of GLUT4 compared with that of GLUT1. The side chains of the amino acid residues that line the glucose permeation pathway along with conformational changes by the transporters themselves most likely control access to the drug binding domain. Mutating two amino acids in GLUT1 to GLUT4 like T30I and H160N might increase access, allowing a small molecule like indinavir to inhibit ATB-BMPA labeling to the same extent as observed for GLUT4. The converse experiment, reducing access to the PI binding site of GLUT4, might require more than just two mutational changes to hinder access of a small inhibitor like indinavir. Converting GLUT1 into GLUT4 using the T30I and H160N double muta-

tion was also observed by the Z-HFFe inhibition of 2-DOG uptake but not with the HR-1 inhibition of ATB-BMPA binding. We speculate that the difference between the Z-HFFe and HR-1 results are primarily due to the difference in size between these two peptides. Z-HFFe and indinavir are similar in size. Interestingly, 2-DOG uptake of all of the chimeric transporters was inhibited by indinavir and Z-HFFe to approximately the same degree. By converting Asn-176 in GLUT4 to His, the inhibition of ATB-BMPA labeling by HR-1 is decreased to the level observed for GLUT1. Indinavir, because of its smaller size, however, can still inhibit ATB-BMPA binding to the same degree as that for GLUT4. Using this same reasoning, substitution of His-160 in GLUT1 to Asn increases accessibility, thereby allowing indinavir but not HR-1 to inhibit ATB-BMPA labeling to a greater extent. These steric influences may at least partially account for the differences observed in the inhibitory potential of different PIs in clinical use. For example, atazanavir, which contains an additional pyridine ring, is known to be a less potent inhibitor of GLUT4 (5).

Overall, the binding experiments appear to be more sensitive than the use of 2-DOG uptake in terms of the detection of subtle changes in the indinavir inhibition. Mutating His-160 to Asn in GLUT1 increased the inhibition of ATB-BMPA labeling but not the inhibition of 2-DOG uptake by indinavir. It was only when the indinavir inhibition of ATB-BMPA labeling increased to a level near that of GLUT4 (GLUT1 T30I and GLUT1 T30I/H160N) that the 2-DOG uptake results mirrored the ATB-BMPA binding results in terms of indinavir inhibition.

Changing Thr-30 to Ile in GLUT1 resulted in a more dramatic alteration in the indinavir inhibition of ATB-BMPA labeling and 2-DOG uptake than mutating His-160 to Asn. Indinavir is not the only compound whose binding to a glucose transporter is affected by the T30I transposition. A pyridylanilinothiazole (STF-31) has recently been shown to specifically target glucose transport through GLUT1 but not GLUT2 in renal cell carcinomas that lack the von Hippel-Lindau tumor suppressor gene resulting in chemical-induced lethality (38). Interestingly, docking of STF-31 to a molecular model of GLUT1showed that Tyr-292, Thr-30, and Thr-295 interact with several moieties of STF-31 (39). Of these amino acids, only Thr-30 is not conserved in GLUT2, an isoform resistant to STF-31. Like GLUT4, GLUT2 is also susceptible to inhibition with indinavir and has an Ile residue corresponding to Thr-30 in GLUT1 (6).

Analysis of the x-ray structure of XylE bound with D-glucose revealed several amino acid residues within the transmembrane permeation pore including Glu-168 (Glu-161 in GLUT1 and Glu-177 in GLUT4) that form hydrogen bonds with the hydroxyl groups of D-glucose (31). ATB-BMPA is a bismannose derivative that can label GLUTs in a D-glucose-inhibitable manner (Fig. 2). Indinavir is a competitive inhibitor of cytoplasmic ATB-BMPA binding. Therefore, it is not unexpected that indinavir would dock within the glucose permeation channel of GLUT4 in close proximity to amino acid residues that participate in glucose binding.

As noted earlier, GLUT1 mutant P385I (P401I in GLUT4) and GLUT4 mutant E409D appear to be locked in an inward facing conformation (27, 28). Interestingly, the recent crystallographic study of XylE has revealed that the corresponding residue of Glu-409 participates in a salt bridge in the partially occluded outward facing conformation and possibly in the partially occluded inward facing conformation (34). This salt bridge is absent when the transporter is in the inward facing conformation. Changing Glu-409 to Asp presumably inhibits salt bridge formation and locks the transporter in an inward facing conformation. The fact that ATB-BMPA labeling of GLUT4 E409D in LDMs is strong and inhibited dramatically with indinavir, D-glucose, and CB indicates that ATB-BMPA can label the transporter from the cytoplasmic side.

A naturally occurring mutation changing the corresponding residue of Pro-401 in GLUT2 to Leu is an inactivating mutation associated with Fanconi-Bickel syndrome (40). In our study, this same mutation in GLUT4 resulted in robust ATB-BMPA labeling of GLUT4 in LDMs that was sensitive to indinavir and D-glucose inhibition but with impaired CB inhibition compared with the GLUT4 E409D results. It is not surprising that the inhibition of ATB-BMPA labeling with CB is altered because Trp-404 in GLUT4, an amino acid that is vital to CB transporter binding, is located only three residues from Pro-401 (29). In addition, changing Pro-401 to Leu/Ile is a dramatic change that reduces the flexibility in helix 10, which is critical for transporter function. The kinking of helix 10 due to prolines 383, 385, and 387 along with glycines 382 and 384 is necessary for the conformational changes that occur during the transition from exofacial to endofacial (or vice versa) glucose binding (34). It was observed that changing the corresponding residue of Pro-401 in GLUT1 to glycine, which still allows conformational flexibility, resulted in a milder effect (27). The fact that inhibition of ATB-BMPA labeling in the GLUT4 P401L mutant is much greater with indinavir than CB is again consistent with our observation that the amino acid side chains directly involved in indinavir/HR-1 and CB binding are distinct. Our CB results for this mutant differ from the original study that reported that changing the corresponding residue of Pro-401 in GLUT1 to Ile resulted in negligible transporter activity and exofacial ATB-BMPA labeling but normal CB binding (27). It seems unlikely that the difference between Ile and Leu, a very conservative change, or the difference in transporter isoform (GLUT1 *versus* GLUT4) would explain the difference with the CB results. The earlier study measured the binding of [^{3}H]CB to GLUT1 P385I (corresponds to GLUT4 P401I) directly, whereas we measured the inhibition of ATB-BMPA labeling by CB. One possibility is that if the amount of [^{3}H]CB used in the original binding study was at saturation a reduction in the affinity in CB binding by changing P401I may not be observed. In our current study, CB still inhibits ATB-BMPA labeling but not as efficiently, indicating that CB does bind to some extent to GLUT4 P401L. Binding of CB to GLUT4 P401L in our study may be further reduced because CB and ATB-BMPA are both competing for transporter binding. In any case, the GLUT4 P401L results further support the conclusion that ATB-BMPA can label GLUTs from the endofacial transporter surface.

Although the current study is directed toward characterizing the effects of the first generation PI indinavir and peptides containing similar structural features, these results can be used as a framework for investigating a wide array of existing and new

drugs for their ability to target these two transporters. Although several of the reported drugs or compounds discussed above such as indinavir and forskolin are selective for GLUT4 over GLUT1, GLUT1 is much more sensitive to inhibition by STF-31 (38) and pentobarbital (41) compared with other GLUTs, suggesting that it may be possible to identify isoform-selective antagonists for many of the GLUT isoforms. Similar to the success in rationally designing the PIs based upon detailed knowledge of the crystal structure of the HIV-1 protease, any advance in determining the tertiary structure of the GLUTs will aid efforts to similarly target the glucose transporters. Selective GLUT antagonists may prove useful as tools to determine the functional role of these proteins in diseases like GLUT1 deficiency syndrome that are caused or contributed by defective glucose transport and to develop novel treatment strategies (42). As recently shown for multiple myeloma (43), targeted disruption of transport may also be useful in treating tumors that depend upon glucose metabolism.

Taken together, characterization of the relative abilities of indinavir, Z-HFFe, and HR-1 to block ATB-BMPA binding and 2-DOG uptake of GLUT1/GLUT4 chimeric transporters identified Thr-30 and His-160 in GLUT1 as amino acid residues that interfere with the ability of PIs to interact with GLUTs and further confirms that the determinants of CB and PI binding are distinct. Our novel use of ATB-BMPA in photolabeling the transporter in an inverted orientation relative to the plasma membrane should prove useful in future studies directed toward probing the cytosolic portion of the glucose permeation pathway. With further advances in the determination of GLUT tertiary structure, these data can serve as a framework for the rational design of isoform-selective glucose transport antagonists and newer PIs that do not contribute to the development of insulin resistance in treated patients.

Acknowledgment—We thank Constanze Haufe for assisting in the construction of several chimeric GLUTs.

REFERENCES

1. Mueckler, M., Caruso, C., Baldwin, S. A., Panico, M., Blench, I., Morris, H. R., Allard, W. J., Lienhard, G. E., and Lodish, H. F. (1985) Sequence and structure of a human glucose transporter. *Science* **229,** 941–945
2. Bogan, J. S. (2012) Regulation of glucose transporter translocation in health and diabetes. *Annu. Rev. Biochem.* **81,** 507–532
3. Hruz, P. W., and Mueckler, M. M. (2001) Structural analysis of the GLUT1 facilitative glucose transporter (review). *Mol. Membr. Biol.* **18,** 183–193
4. Murata, H., Hruz, P. W., and Mueckler, M. (2000) The mechanism of insulin resistance caused by HIV protease inhibitor therapy. *J. Biol. Chem.* **275,** 20251–20254
5. Hresko, R. C., and Hruz, P. W. (2011) HIV Protease inhibitors act as competitive inhibitors of the cytoplasmic glucose binding site of GLUTs with differing affinities for GLUT1 and GLUT4. *PLoS One* **6,** e25237
6. Murata, H., Hruz, P. W., and Mueckler, M. (2002) Indinavir inhibits the glucose transporter isoform Glut4 at physiologic concentrations. *AIDS* **16,** 859 – 863
7. Hruz, P. W. (2011) Molecular mechanisms for insulin resistance in treated HIV-infection. *Best Pract. Res. Clin. Endocrinol. Metab.* **25,** 459 – 468
8. Hruz, P. W., Yan, Q., Tsai, L., Koster, J., Xu, L., Cihlar, T., and Callebaut, C. (2011) GS-8374, a novel HIV protease inhibitor, does not alter glucose homeostasis in cultured adipocytes or in a healthy-rodent model system. *Antimicrob. Agents Chemother.* **55,** 1377–1382
9. Rudich, A., Konrad, D., Török, D., Ben-Romano, R., Huang, C., Niu, W., Garg, R. R., Wijesekara, N., Germinario, R. J., Bilan, P. J., and Klip, A. (2003) Indinavir uncovers different contributions of GLUT4 and GLUT1 towards glucose uptake in muscle and fat cells and tissues. *Diabetologia* **46,** 649 – 658
10. Hruz, P. W., and Yan, Q. (2006) Tipranavir without ritonavir does not acutely induce peripheral insulin resistance in a rodent model. *J. Acquir. Immune Defic. Syndr.* **43,** 624 – 625
11. Hertel, J., Struthers, H., Horj, C. B., and Hruz, P. W. (2004) A structural basis for the acute effects of HIV protease inhibitors on GLUT4 intrinsic activity. *J. Biol. Chem.* **279,** 55147–55152
12. Koumanov, F., Yang, J., Jones, A. E., Hatanaka, Y., and Holman, G. D. (1998) Cell-surface biotinylation of GLUT4 using bis-mannose photolabels. *Biochem. J.* **330,** 1209 –1215
13. Hresko, R. C., Crankshaw, C. L., and Hruz, P. W. (2011) Photolabeling of the endofacial glucose binding site of GLUT4 with biotinylated ATB-BMPA and WUCC2, a novel FLAG-tagged peptide. *Diabetes* **60 Supplement 1,** A409
14. Noel, L. E., and Newgard, C. B. (1997) Structural domains that contribute to substrate specificity in facilitated glucose transporters are distinct from those involved in kinetic function: studies with GLUT-1/GLUT-2 chimeras. *Biochemistry* **36,** 5465–5475
15. Czech, M. P., Chawla, A., Woon, C. W., Buxton, J., Armoni, M., Tang, W., Joly, M., and Corvera, S. (1993) Exofacial epitope-tagged glucose transporter chimeras reveal COOH-terminal sequences governing cellular localization. *J. Cell Biol.* **123,** 127–135
16. De Zutter, J. K., Levine, K. B., Deng, D., and Carruthers, A. (2013) Sequence determinants of GLUT1 oligomerization: analysis by homology-scanning mutagenesis. *J. Biol. Chem.* **288,** 20734 –20744
17. Ory, D. S., Neugeboren, B. A., and Mulligan, R. C. (1996) A stable human-derived packaging cell line for production of high titer retrovirus/vesicular stomatitis virus G pseudotypes. *Proc. Natl. Acad. Sci. U.S.A.* **93,** 11400 –11406
18. Wang, W., and Malcolm, B. A. (1999) Two-stage PCR protocol allowing introduction of multiple mutations, deletions and insertions using QuikChange site-directed mutagenesis. *BioTechniques* **26,** 680 – 682
19. Tordjman, K. M., Leingang, K. A., James, D. E., and Mueckler, M. M. (1989) Differential regulation of two distinct glucose transporter species expressed in 3T3-L1 adipocytes: effect of chronic insulin and tolbutamide treatment. *Proc. Natl. Acad. Sci. U.S.A.* **86,** 7761–7765
20. Piper, R. C., Hess, L. J., and James, D. E. (1991) Differential sorting of two glucose transporters expressed in insulin-sensitive cells. *Am. J. Physiol.* **260,** C570 –C580
21. Sievers, F., Wilm, A., Dineen, D., Gibson, T. J., Karplus, K., Li, W., Lopez, R., McWilliam, H., Remmert, M., Söding, J., Thompson, J. D., and Higgins, D. G. (2011) Fast, scalable generation of high-quality protein multiple sequence alignments using ClustalΩ. *Mol. Syst. Biol.* **7,** 539
22. Caffrey, D. R., Dana, P. H., Mathur, V., Ocano, M., Hong, E. J., Wang, Y. E., Somaroo, S., Caffrey, B. E., Potluri, S., and Huang, E. S. (2007) PFAAT version 2.0: a tool for editing, annotating, and analyzing multiple sequence alignments. *BMC Bioinformatics* **8,** 381
23. Trott, O., and Olson, A. J. (2010) AutoDock Vina: improving the speed and accuracy of docking with a new scoring function, efficient optimization, and multithreading. *J. Comput. Chem.* **31,** 455– 461
24. Gorga, F. R., and Lienhard, G. E. (1981) Equilibria and kinetics of ligand binding to the human erythrocyte glucose transporter. Evidence for an alternating conformation model for transport. *Biochemistry* **20,** 5108 –5113
25. Smirnova, I., Kasho, V., and Kaback, H. R. (2011) Lactose permease and the alternating access mechanism. *Biochemistry* **50,** 9684 –9693
26. Clark, A. E., and Holman, G. D. (1990) Exofacial photolabelling of the human erythrocyte glucose transporter with an azitrifluoroethylbenzoyl-substituted bismannose. *Biochem. J.* **269,** 615– 622
27. Tamori, Y., Hashiramoto, M., Clark, A. E., Mori, H., Muraoka, A., Kadowaki, T., Holman, G. D., and Kasuga, M. (1994) Substitution at Pro^{385} of GLUT1 perturbs the glucose transport function by reducing conformational flexibility. *J. Biol. Chem.* **269,** 2982–2986
28. Schürmann, A., Doege, H., Ohnimus, H., Monser, V., Buchs, A., and Joost,

H. G. (1997) Role of conserved arginine and glutamate residues on the cytosolic surface of glucose transporters for transporter function. *Biochemistry* **36,** 12897–12902
29. Inukai, K., Asano, T., Katagiri, H., Anai, M., Funaki, M., Ishihara, H., Tsukuda, K., Kikuchi, M., Yazaki, Y., and Oka, Y. (1994) Replacement of both tryptophan residues at 388 and 412 completely abolished cytochalasin B photolabelling of the GLUT1 glucose transporter. *Biochem. J.* **302,** 355–361
30. Holman, G. D., Kozka, I. J., Clark, A. E., Flower, C. J., Saltis, J., Habberfield, A. D., Simpson, I. A., and Cushman, S. W. (1990) Cell surface labeling of glucose transporter isoform GLUT4 by bis-mannose photolabel. Correlation with stimulation of glucose transport in rat adipose cells by insulin and phorbol ester. *J. Biol. Chem.* **265,** 18172–18179
31. Sun, L., Zeng, X., Yan, C., Sun, X., Gong, X., Rao, Y., and Yan, N. (2012) Crystal structure of a bacterial homologue of glucose transporters GLUT1-4. *Nature* **490,** 361–366
32. Mueckler, M., and Makepeace, C. (2009) Model of the exofacial substrate-binding site and helical folding of the human Glut1 glucose transporter based on scanning mutagenesis. *Biochemistry* **48,** 5934–5942
33. Mueckler, M., Weng, W., and Kruse, M. (1994) Glutamine 161 of Glut1 glucose transporter is critical for transport activity and exofacial ligand binding. *J. Biol. Chem.* **269,** 20533–20538
34. Quistgaard, E. M., Löw, C., Moberg, P., Trésaugues, L., and Nordlund, P. (2013) Structural basis for substrate transport in the GLUT-homology family of monosaccharide transporters. *Nat. Struct. Mol. Biol.* **20,** 766–768
35. Iancu, C. V., Zamoon, J., Woo, S. B., Aleshin, A., and Choe, J. Y. (2013) Crystal structure of a glucose/H^+ symporter and its mechanism of action. *Proc. Natl. Acad. Sci. U.S.A.* **110,** 17862–17867
36. Hellwig, B., and Joost, H. G. (1991) Differentiation of erythrocyte-(GLUT1), liver-(GLUT2), and adipocyte-type (GLUT4) glucose transporters by binding of the inhibitory ligands cytochalasin B, forskolin, dipyridamole, and isobutylmethylxanthine. *Mol. Pharmacol.* **40,** 383–389
37. Lachaal, M., Rampal, A. L., Lee, W., Shi, Y., and Jung, C. Y. (1996) GLUT1 transmembrane glucose pathway. Affinity labeling with a transportable D-glucose diazirine. *J. Biol. Chem.* **271,** 5225–5230
38. Chan, D. A., Sutphin, P. D., Nguyen, P., Turcotte, S., Lai, E. W., Banh, A., Reynolds, G. E., Chi, J.-T., Wu, J., Solow-Cordero, D. E., Bonnet, M., Flanagan, J. U., Bouley, D. M., Graves, E. E., Denny, W. A., Hay, M. P., and Giaccia, A. J. (2011) Targeting GLUT1 and the Warburg effect in renal cell carcinoma by chemical synthetic lethality. *Sci. Transl. Med.* **3,** 94ra70
39. Madej, M. G., Sun, L., Yan, N., and Kaback, H. R. (2014) Functional architecture of MFS D-glucose transporters. *Proc. Natl. Acad. Sci. U.S.A.* **111,** E719–E727
40. Michau, A., Guillemain, G., Grosfeld, A., Vuillaumier-Barrot, S., Grand, T., Keck, M., L'Hoste, S., Chateau, D., Serradas, P., Teulon, J., De Lonlay, P., Scharfmann, R., Brot-Laroche, E., Leturque, A., and Le Gall, M. (2013) Mutations in SLC2A2 reveal hGLUT2 function in pancreatic beta cell development. *J. Biol. Chem.* **288,** 31080–31092
41. Haspel, H. C., Stephenson, K. N., Davies-Hill, T., El-Barbary, A., Lobo, J. F., Croxen, R. L., Mougrabi, W., Koehler-Stec, E. M., Fenstermacher, J. D., and Simpson, I. A. (1999) Effects of barbiturates on facilitative glucose transporters are pharmacologically specific and isoform selective. *J. Membr Biol.* **169,** 45–53
42. Klepper, J., and Leiendecker, B. (2007) GLUT1 deficiency syndrome—2007 update. *Dev. Med. Child Neurol.* **49,** 707–716
43. McBrayer, S. K., Cheng, J. C., Singhal, S., Krett, N. L., Rosen, S. T., and Shanmugam, M. (2012) Multiple myeloma exhibits novel dependence on GLUT4, GLUT8, and GLUT11: implications for glucose transporter-directed therapy. *Blood* **119,** 4686–4697